PROCEEDINGS OF SPIE

Generation and recombination of free carriers in silicon nano-waveguides

Dainese, Paulo, Aldaya, Ivan, Gil-Molina, Andrés, Gabrielli, Lucas, Fragnito, Hugo, et al.

Generation and recombination of free-carriers in silicon nano-waveguides

Paulo Dainese[a,b], Ivan Aldaya[c,b], Andres Gil-Molina[b], Lucas H. Gabrielli[b], Hugo L. Fragnito[d,b], and Julian L. Pita[b]

[a]Corning Research and Development Corporation, One Science Drive, Corning, NY, USA
[b]University of Campinas, Cidade Universitária Zeferino Vaz, Campinas, SP, Brazil
[c]State University of São Paulo, Profa. Isette Corrêa Fontão, São João da Boa Vista, SP, Brazil
[d]Mackenzie Presbiterian University, R. Maria Antônia, São Paulo, SP, Brazil

ABSTRACT

Generation and recombination of free carriers in silicon photonics is fundamental to understand several nonlinear optical phenomena and engineer novel devices. Particularly in strip nano-waveguides, the tightly confined optical field results in highly efficient generation of free-carriers, both through linear and nonlinear absorption. Furthermore, the large surface-to-volume ratio results in a nonlinear recombination behavior dominated by a trap-assisted mechanism. Through time-resolved pump-and-probe experiments, we performed a detailed experimental characterization of linear and nonlinear generation rates, as well as recombination dynamics. We developed analytical expressions to determine the carrier density averaged along the waveguide from the measured free-carrier absorption for different input pump power levels. As a result, we were able to discriminate the contributions from two-photon absorption (TPA) and single-photon absorption (SPA), obtaining absorption coefficients of (1.5 ± 0.1) cm/GW and (1.9 ± 0.1) m^{-1}, respectively. Our results then reveal that the effective TPA within the waveguide is higher than the value reported for bulk silicon, and that SPA plays an important role in carrier generation up to $\approx$300 mW. With regards to recombination dynamics, our results show a highly nonlinear decay curve with instantaneous carrier lifetime varying as the recombination evolves (initially faster with lifetime of $\sim$800 ps and slower at final stages of the decay, reaching $\sim$300 ns). We interpret our results with a theoretical framework based on trap-assisted recombination statistics applied to strip nano-waveguides, and explore its implication to the dynamics of nonlinear nanophotonic devices in which free carriers play a critical role.

Keywords: Semiconductor, silicon photonics, two-photon absorption, free-carrier generation, free-carrier recombination

1. INTRODUCTION

Silicon-on-insulator (SOI) has emerged as a high potential technology for future integrated optical systems due to its compatibility with the widely-employed complimentary metal oxide semiconductor (CMOS) fabrication process.[1–3] SOI technology is also interesting because the large refractive index contrast between the core (silicon) and cladding (glass/air) leads to strong light confinement, enabling compact devices and, along with silicon's high nonlinear coefficient, making this platform attractive for implementing nonlinear devices.[4,5] The presence of free carriers within the guiding structure, however, poses a critical challenge to the design of such devices.[6–9] Free carriers interact with the optical mode by modifying both the real and imaginary parts of the core refractive index, so-called free-carrier dispersion (FCD) and free-carrier absorption (FCA) effects, respectively.[10] In addition, heat generation due to non-radiative carrier recombination modifies the refractive index through the thermo-optic effect.[11] The combination of these effects can result in instabilities in resonant structures as reported in [12]. FCA, FCD, and thermal effect, however, can also be exploited as light control mechanisms. For instance, in [13], FCD is employed to shift the resonance in a micro-ring resonator, whereas in [14], FCA is

---

Correspondence: dainesep@corning.com

used to compress optical pulses. An accurate knowledge of free-carrier dynamics is then critical to understand the response of fabricated devices, predict operation limits, and improve future designs.

In general, carrier dynamics depends on (i) generation, (ii) diffusion and (iii) recombination mechanisms. In the particular case of the widely employed strip nano-waveguides, all-optical generation of free-carriers is of great importance for nonlinear applications. Given the 1.1-eV bandgap of silicon, carrier generation at 1550 nm is attributed to two-photon absorption (TPA).[15, 16] However, the presence of intra-bandgap states due to defects or impurities can result in non-negligible single-photon absorption (SPA), further contributing to free-carrier generation. Another relevant aspect of carrier generation in strip nano-waveguides is an effective enhancement of the nonlinear TPA coefficient in the strong guidance regime.[17–19] These two aspects, the presence of both SPA and TPA and an enhancement of the effective TPA coefficient, motivate the present detailed characterization of all-optical carrier generation in silicon nano-waveguides. An additional aspect particular to strip waveguides is that diffusion out of the silicon core cannot happen as it is completely surrounded by oxide (or air). This means that once free-carriers are generated, they are tightly confined into the core and continuously interact with the optical mode until completely recombined back into the valence band. Recombination can occur through several mechanisms such as radiative, Auger and trap-assisted recombination.[20] The indirect bandgap of silicon strongly reduces radiative recombination, while Auger processes are significant only for relatively high carrier densities, typically above 10^{18} cm^{-3}.[21] It is expected therefore that in this kind of waveguides carrier recombination is dominated by trap-assisted, usually described by the standard Shockley-Read-Hall (SRH) model.[22] The most common regime generally observed in SRH recombination in bulk or large cross-section waveguides is that governed by small trap density relative to excess carriers. We observe in our experiments, however, that the recombination dynamics in nano-strip waveguides follows a more complex dynamics better explained by large trap density regime, which causes significant unbalance between free electrons and free holes.[23] One of the consequence of the large trap density regime is the fact that carrier lifetime is not only dependent on the instantaneous carrier density but also on the previous carrier densities.

In this paper we summarize our results presented in [24] and [25], covering both generation as well as recombination mechanisms, and discuss its applications to all-optical switching. The presented characterization of the commonly used 220 nm×450 nm provides a deeper understanding of the complex carrier dynamics and our results can be used to model device performance in similar structures. The paper is organized as follows: in Section 2, we describe the employed experimental setup while, in Section 3, we present the characterization results of both carrier generation and recombination. In Section 4 we analyze the effect of the carrier dynamics on the optical control of light. Finally, Section 5 concludes the paper.

2. EXPERIMENTAL SETUP AND SAMPLES

In Fig. 1(a) we present the general block diagram of the pump-and-probe experimental setup used to study free-carrier generation and recombination processes in silicon nano-waveguides. For the pump, we used a train of optical pulses tuned at 1549 nm, of short duration (nearly 100 ps) and a repetition rate of 500 kHz. Short
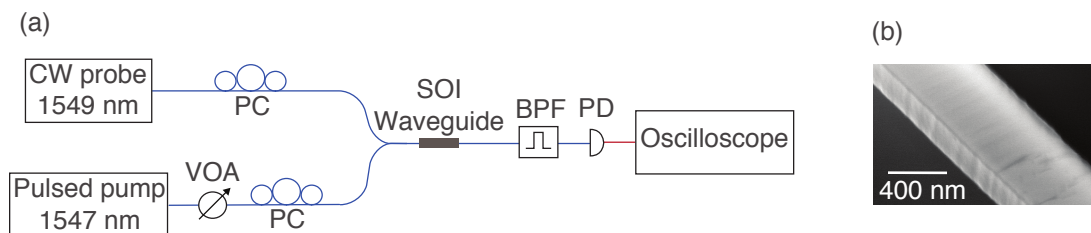

Figure 1: (a) Block diagram of the employed experimental setup. VOA: variable optical attenuator, PC: polarization controller, BPF: bandpass filter, PD: photodetector. (b) SEM image of a SOI waveguide similar to that characterized in this work (in order to avoid charging, SEM image was taken using an unclad waveguide).

pulses were employed because carrier lifetime can be as fast as ~800 ps, whereas the low-repetition rate was required to minimize the influence of (pulse-to-pulse) accumulation of free carriers in our measurements. The power of the pump was controlled by means of a variable optical attenuator (VOA), being able to vary the pump power from few mW up to 1 W without modifying the main characteristics of the pulse shape. For the probe, we used a continuous wave (CW) laser tuned at 1547 nm. The probe power was kept as low as ~50 μW in order to ensure minimal contribution to the free-carrier density. The pump and probe signals were combined via a fiber coupler before being injected into the SOI waveguide through a diffraction grating. Since the grating couplers were design to efficiently couple only the quasi-traversal electric (TE) mode of the SOI waveguide, we used polarization controllers (PCs) to optimize the coupling of both the pump and the probe by modifying their states of polarization. After propagating over the SOI waveguide, the pump and probe signals were coupled back to an optical fiber by using a second diffraction grating. The probe signal was then separated from the pump by an optical bandpass filter (BPF) and detected by an oscilloscope equipped with a built-in photodetector (PD) of 28-GHz bandwidth. A detailed description of the experimental setup can be found in [24].

The samples analyzed in this work were SOI strip waveguides with silica cladding and a cross-section of 450 nm×220 nm. The waveguides were fabricated at imec/Europractice using optical lithography and inductively coupled plasma reactive ion etching. In Fig. 1(b) we present a scanning-electron microscope (SEM) image of an unclad SOI strip waveguide (similar to the samples used in our experiments, but before silica deposition). We performed the linear regression of the transmittances of three samples with different lengths (i.e., 2.4, 5.9, and 30 mm), resulting in a propagation loss of ~1.4 dB/cm and a fiber-to-grating coupling loss of ~3.4 dB.

3. FREE-CARRIER DYNAMICS IN SILICON NANO-WAVEGUIDES

3.1 Generation through SPA and TPA

Figure 2(a) shows the normalized probe transmittance for three different pump power levels, which account for losses induced by the pump via non-degenerate TPA and FCA. The signal to noise ratio of the normalized transmittance curves has been enhanced by averaging several traces, being the number of averaged traces dependent on the pumping power. In Fig. 2(a) we can identify an initial regime dominated by non-degenerate TPA and characterized by a fast drop in the normalized transmittance. This stage is followed by a slower regime dominated by FCA resulting from the free carriers generated along the waveguide. From inspection, we set the transition between both regimes at around $t_0 = 100$ ps after the peak of the pump pulse, considering that at this time non-degenerate TPA no longer contributes significantly. From the measured non-linear loss at $t_0 =$, the
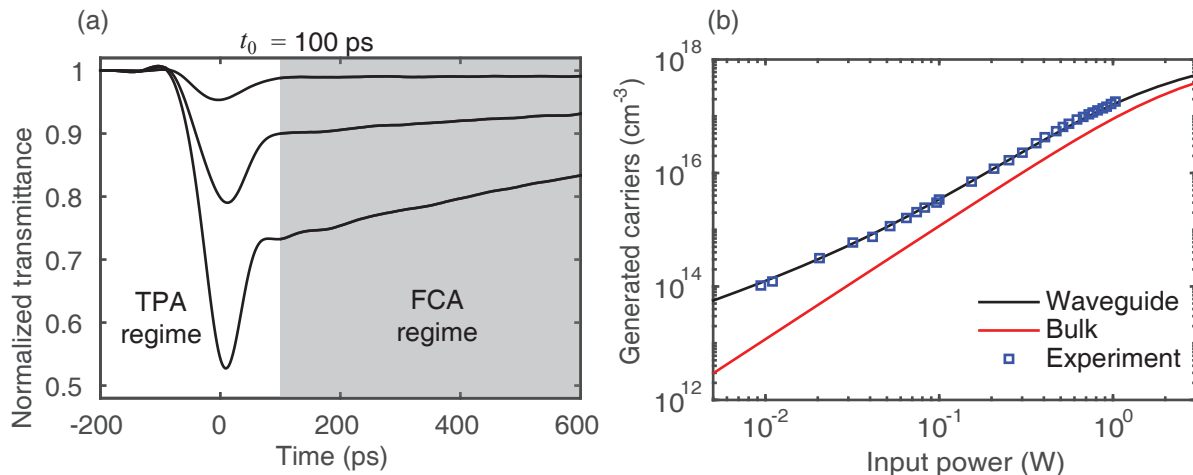

Figure 2: (a) Normalized probe transmittance for 80-ps pump pulses with different peak power levels (100, 360 and 670 mW). The regimes dominated by TPA and FCA (shadowed area) can be identified. (b) Comparison between free-carrier generation in waveguide and bulk in terms of the input power.

generated free-carrier density can be directly obtained.[25] In Fig. 2(b) we present the generated carrier density as a function of the input pump power (square symbols). The red curve represents the predicted carrier density considering only TPA with a coefficient of 0.7 cm/GW, which clearly does not agree with the experimental observation. At low power the experimental result reveals a *lower* slope, indicating presence of SPA. At high power, the observed carrier density is dominated by TPA but is clearly shifted upwards from the predicted curve, indicating an enhanced effective TPA coefficient. In [25], we developed analytical expressions that relate both SPA and TPA coefficients with the generated carrier density as a function of the input power. The measured SPA and TPA coefficients of the tested waveguide were α_{SPA} =(1.9±0.1) m^{-1} and β_{TPA} =(1.5±0.1) cm/GW. The black curve in Fig. 2(b) shows the calculated carrier density using the measured parameters, and is in good agreement with the experimental data. From our results, we can point out two main observations. On the one hand, although the measured SPA corresponds to approximately 6% of the total propagation loss ($\sim$ 1.4 dB/cm), it has a significant contribution in carrier generation for low and intermediate power levels (up to ≈300 mW). On the other hand, the measured TPA corresponds to a larger value than those previously reported for bulk silicon, which are within the range of 0.4 to 1.2 cm/GW.[15, 26, 27] Theoretically, based on the model presented in [18, 19], we calculated that the effective TPA coefficient is enhanced in the tight optical confining nano-waveguide by ≈20% compared to bulk silicon, which is inline with our observation of 1.5 cm/GW.

3.2 Recombination dynamics

The results presented so far on the generation of free-carriers were based on measuring the carrier density at $t_0 =$ 100 ps in the transmittance curves in Fig. 2(a), just after the pulse. Beyond this point, no further generation occurs and the carrier density decays due to recombination. Figure 3(a) shows the extracted time-resolved carrier densities for pump pulse power levels of 0.07 W, 0.28 W, and 0.83 W at the waveguide input. Note a much longer time scale than that presented in Fig. 2(a). Comparing the obtained traces, there are several points that should be noted. First, there is a significant change on the slope as the recombination evolves. Considering the logarithmic scale, this changing slope indicates that the *instantaneous* carrier lifetime ($\tau_c(t) = -N \cdot (dN/dt)^{-1}$) varies as the recombination evolves in time. Second, it is clear that for a given carrier density, the slopes of the different traces are different. This shows that the carrier lifetime is not fully determined by the instantaneous carrier density (which should have been the case in the small trap density regime in SRH recombination). An additional point to highlight is that at the initial stage of the recombination, the slopes of the different traces for the different considered pump power levels converge. These observations can be quantitatively assessed by
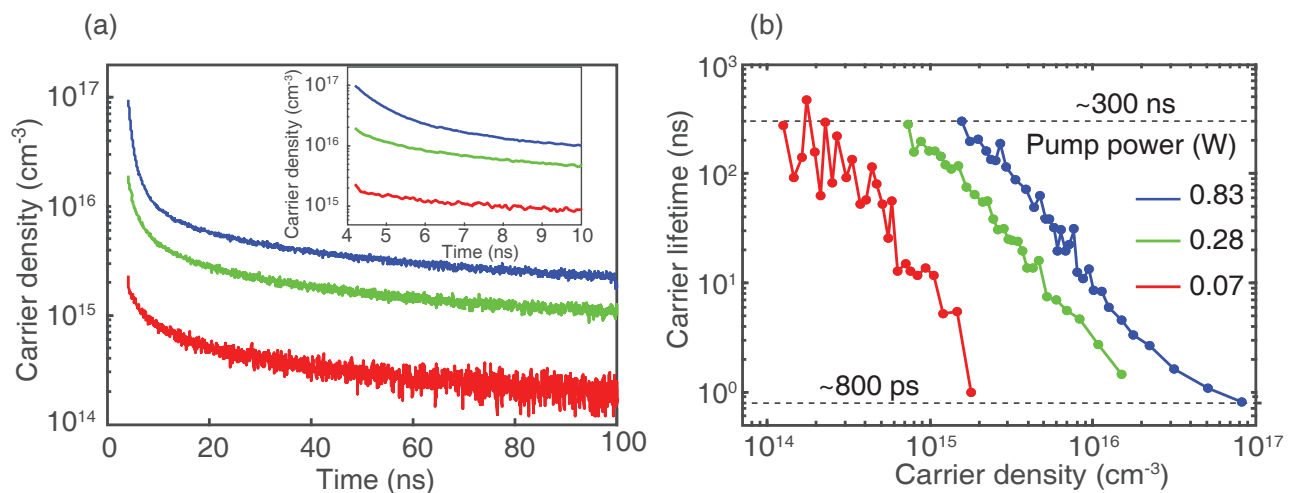

Figure 3: (a) Time-resolved carrier density for different pump power levels. The inset shows a zoom of the initial stage after the pulse. (b) Extracted carrier lifetime in terms of the carrier density for the same pump power levels.
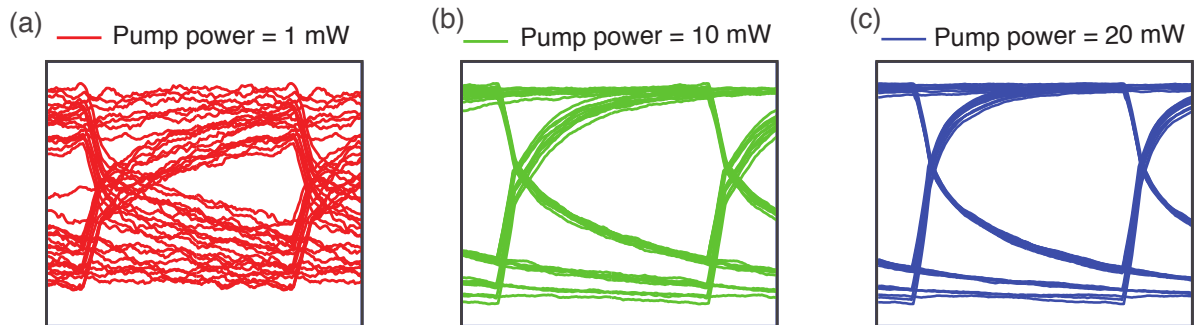
Figure 4: Eye diagrams of the probe output for different pump power levels: (a) 1 mW, (b) 10 mW, and (c) 20 mW.

plotting the instantaneous carrier lifetime in terms of the carrier density, as shown in Fig. 3(b). As indicated, the carrier lifetime is not uniquely determined by the instantaneous density. It is important to note that, even if the shortest ($\sim$800 ps) and the longest carrier lifetimes ($\sim$ 300 ns) are similar for the different pump power levels, the relation between carrier density and lifetime is dependent on the input pump power due to the different initial carrier densities. Simulation results presented in [24] reveal that when trap density is large, the observations presented here can be well explained. Physically, a large density of empty traps quickly capture free electrons causing the initial fast drop in the nonlinear absorption and leaving a large unbalance between free electrons and free holes. Slowly, hole recombination follows until all free carriers are recombined and the nonlinear loss ceases.

4. ALL-OPTICAL CONTROL

Once the carrier generation and recombination dynamics were studied, the system response under pseudorandom operation was analyzed. That is, instead of a single pulse, a pseudorandom bit sequence was employed as pump. Thus, the objective is not to characterize the carrier recombination process but to evaluate the performance of an all-optical non-parametric optical switch. Figure 4 shows the eye diagrams for the probe output when the pump power is (a) 1 mW, (b) 10 mW, and (c) 20 mW. As expected from the previous recombination time analysis, higher pump power results in a faster device. However, due to the highly nonlinear recombination dynamics, the system response is word-dependent. All the three eye diagrams shown in Fig. 4(a), (b), and (c) present both horizontal and vertical asymmetry. The lack of horizontal symmetry indicates that the system is bandwidth limited, whereas the vertical asymmetry means that the rising and falling times are different, which does not occur in linear and time-invariant systems. However, even if the system is band-limited for the three pump-power levels, it is clear that for 10 and 20 mW, the vertical opening of the eye diagram is significantly better.

5. CONCLUSIONS

In this paper the generation and recombination of free carriers in a silica cladded strip SOI waveguide are characterized. Results from time-resolved pump-and-probe experiments reveal that the generated carrier density is higher in waveguides than in bulk silicon due an enhanced effective TPA as well as the presence of non-negligible SPA. We have also observed recombination dynamics representative of large trap state density regime. The higher carrier generation and complex recombination dynamics should then be considered in the design of new devices, specially in nonlinear applications where moderate or high optical densities are required.

REFERENCES

[1] Jalali, B. and Fathpour, S., "Silicon photonics," *Journal of Lightwave Technology* **24**(12), 4600–4615 (2006).

[2] Pavesi, D., "Silicon fundamentals for photonics applications," *Silicon Photonics* , 2000–2000 (2004).

[3] Soref, R., "The past, present, and future of silicon photonics," *IEEE Journal of Selected Topics in Quantum Electronics* **12**(6), 1678–1687 (2006).

[4] Leuthold, J., Koos, C., and Freude, W., "Nonlinear silicon photonics," *Nature Photonics* **4**(8), 535 (2010).

[5] Huang, Y., Cazzanelli, M., Sang, X., and Boyraz, O., "Nonlinear optics in silicon," in [*Handbook of Silicon Photonics*], 212–263, CRC Press (2016).

[6] Blanco-Redondo, A., Husko, C., Eades, D., Zhang, Y., Li, J., Krauss, T., and Eggleton, B., "Observation of soliton compression in silicon photonic crystals," *Nature Communications* **5**, 3160 (2014).

[7] Leo, F., Gorza, S.-P., Coen, S., Kuyken, B., and Roelkens, G., "Coherent supercontinuum generation in a silicon photonic wire in the telecommunication wavelength range," *Optics Letters* **40**(1), 123–126 (2015).

[8] Liang, T. and Tsang, H., "Role of free carriers from two-photon absorption in Raman amplification in silicon-on-insulator waveguides," *Applied Physics Letters* **84**(15), 2745–2747 (2004).

[9] Shin, H., Qiu, W., Jarecki, R., Cox, J. A., Olsson III, R. H., Starbuck, A., Wang, Z., and Rakich, P. T., "Tailorable stimulated Brillouin scattering in nanoscale silicon waveguides," *Nature Communications* **4**, 1944 (2013).

[10] Soref, R. and Bennett, B., "Electrooptical effects in silicon," *IEEE Journal of Quantum Electronics* **23**(1), 123–129 (1987).

[11] Bogaerts, W., Fiers, M., and Dumon, P., "Design challenges in silicon photonics," *IEEE Journal of Selected Topics in Quantum Electronics* **20**(4), 1–8 (2014).

[12] Pernice, W. H., Li, M., and Tang, H. X., "Time-domain measurement of optical transport in silicon microring resonators," *Optics Express* **18**(17), 18438–18452 (2010).

[13] Almeida, V. R., Barrios, C. A., Panepucci, R. R., and Lipson, M., "All-optical control of light on a silicon chip," *Nature* **431**(7012), 1081 (2004).

[14] Tien, E.-K., Yuksek, N. S., Qian, F., and Boyraz, O., "Pulse compression and modelocking by using TPA in silicon waveguides," *Optics Express* **15**(10), 6500–6506 (2007).

[15] Bristow, A. D., Rotenberg, N., and Van Driel, H. M., "Two-photon absorption and Kerr coefficients of silicon for 850–2200 nm," *Applied Physics Letters* **90**(19), 191104 (2007).

[16] Lin, Q., Painter, O. J., and Agrawal, G. P., "Nonlinear optical phenomena in silicon waveguides: modeling and applications," *Optics Express* **15**(25), 16604–16644 (2007).

[17] Zhang, Y., Husko, C., Lefrancois, S., Rey, I. H., Krauss, T. F., Schröder, J., and Eggleton, B. J., "Nondegenerate two-photon absorption in silicon waveguides: analytical and experimental study," *Optics Express* **23**(13), 17101–17110 (2015).

[18] Afshar, S. and Monro, T. M., "A full vectorial model for pulse propagation in emerging waveguides with subwavelength structures part i: Kerr nonlinearity," *Optics express* **17**(4), 2298–2318 (2009).

[19] Afshar, V. S., Monro, T., and De Sterke, C. M., "Understanding the contribution of mode area and slow light to the effective kerr nonlinearity of waveguides," *Optics express* **21**(15), 18558–18571 (2013).

[20] Schroder, D. K., "Carrier lifetimes in silicon," *IEEE Transactions on Electron Devices* **44**(1), 160–170 (1997).

[21] Sze, S. M. and Ng, K. K., [*Physics of semiconductor devices*], John wiley & sons (2006).

[22] Shockley, W. and Read Jr, W., "Statistics of the recombinations of holes and electrons," *Physical Review* **87**(5), 835 (1952).

[23] Blakemore, J. S., [*Semiconductor statistics*], Courier Corporation (2002).

[24] Aldaya, I., Gil-Molina, A., Pita, J. L., Gabrielli, L. H., Fragnito, H. L., and Dainese, P., "Nonlinear carrier dynamics in silicon nano-waveguides," *Optica* **4**(10), 1219–1227 (2017).

[25] Gil-Molina, A., Aldaya, I., Pita, J. L., Gabrielli, L. H., Fragnito, H. L., and Dainese, P., "Optical free-carrier generation in silicon nano-waveguides at 1550 nm," *Applied Physics Letters* **112**(25), 251104 (2018).

[26] Dinu, M., Quochi, F., and Garcia, H., "Third-order nonlinearities in silicon at telecom wavelengths," *Applied Physics Letters* **82**(18), 2954–2956 (2003).

[27] Tsang, H. K., Wong, C., Liang, T., Day, I., Roberts, S., Harpin, A., Drake, J., and Asghari, M., "Optical dispersion, two-photon absorption and self-phase modulation in silicon waveguides at 1.5μm wavelength," *Applied Physics Letters* **80**(3), 416–418 (2002).